The Astrophysical Journal, 753:82 (9pp), 2012 July 1 doi:10.1088/0004-637X/753/1/82

THE PROPERTIES OF THE 2175 Å EXTINCTION FEATURE DISCOVERED IN GRB AFTERGLOWS

Tayyaba Zafar[1,2], Darach Watson[1], Árdís Elíasdóttir[1], Johan P. U. Fynbo[1], Thomas Krühler[1,3], Patricia Schady[3], Giorgos Leloudas[1], Páll Jakobsson[4], Christina C. Thöne[5], Daniel A. Perley[6], Adam N. Morgan[6], Joshua Bloom[6], and Jochen Greiner[3]

[1] Dark Cosmology Centre, Niels Bohr Institute, University of Copenhagen, Juliane Maries Vej 30, DK-2100 Copenhagen Ø, Denmark; tayyaba@dark-cosmology.dk, darach@dark-cosmology.dk, ardis@dark-cosmology.dk

[2] Laboratoire d'Astrophysique de Marseille - LAM, Université Aix-Marseille & CNRS, UMR7326, 38 rue F. Joliot-Curie, 13388 Marseille Cedex 13, France

[3] Max-Planck Institut für Extraterrestrische Physik, Giessenbachstrasse, 85748, Garching, Germany

[4] Centre for Astrophysics and Cosmology, Science Institute, University of Iceland, Dunhagi 5, IS-107 Reykjavík, Iceland

[5] INAF-Osservatorio Astronomico di Brera, Via Bianchi 46, I-23807, Merate (Lc), Italy

[6] Department of Astronomy, University of California, Berkeley, CA 94720-3411, USA

Received 2011 December 7; accepted 2012 May 1; published 2012 June 15

ABSTRACT

The unequivocal, spectroscopic detection of the 2175 Å bump in extinction curves outside the Local Group is rare. To date, the properties of the bump have been examined in only two gamma-ray burst (GRB) afterglows (GRB 070802 and GRB 080607). In this work, we analyze in detail the detections of the 2175 Å extinction bump in the optical spectra of two further GRB afterglows: GRB 080605 and 080805. We gather all available optical/near-infrared photometric, spectroscopic, and X-ray data to construct multi-epoch spectral energy distributions (SEDs) for both GRB afterglows. We fit the SEDs with the Fitzpatrick & Massa model with a single or broken power law. We also fit a sample of 38 GRB afterglows, known to prefer a Small Magellanic Cloud (SMC)-type extinction curve, with the same model. We find that the SEDs of GRB 080605 and GRB 080805 at two epochs are fit well with a single power law with a derived extinction of $A_V = 0.52^{+0.13}_{-0.16}$ and $0.50^{+0.13}_{-0.10}$, and $2.1^{+0.7}_{-0.6}$ and 1.5 ± 0.2, respectively. While the slope of the extinction curve of GRB 080805 is not well constrained, the extinction curve of GRB 080605 has an unusual very steep far-UV rise together with the 2175 Å bump. Such an extinction curve has previously been found in only a small handful of sightlines in the Milky Way. One possible explanation of such an extinction curve may be dust arising from two different regions with two separate grain populations, however we cannot distinguish the origin of the curve. We finally compare the four 2175 Å bump sightlines to the larger GRB afterglow sample and to Local Group sightlines. We find that while the width and central positions of the bumps are consistent with what is observed in the Local Group, the relative strength of the detected bump ($A_{\rm bump}$) for GRB afterglows is weaker for a given A_V than for almost any Local Group sightline. Such dilution of the bump strength may offer tentative support to a dual dust-population scenario.

Key words: dust, extinction – gamma-ray burst: general – gamma-ray burst: individual (GRB 080605, GRB 080805)

Online-only material: color figures

1. INTRODUCTION

Starlight in galaxies is absorbed and scattered by dust grains present in the interstellar medium (ISM). The process is usually quantified by the introduction of an interstellar extinction curve. A characteristic feature in the extinction curves of the Milky Way (MW) and Large Magellanic Cloud (LMC) is the 2175 Å extinction bump, first discovered by Stecher (1965). The 2175 Å bump has been attributed to absorption by graphite grains processed by star formation (e.g., Draine 2003). However, the exact origin of the 2175 Å bump is still unclear although several candidates have been suggested ranging from carbonaceous materials (Henrard et al. 1997) to iron-poor silicates in the form of partially hydrogenated amorphous Mg_2SiO_4 particles (Steel & Duley 1987). It has also been suggested that coating on graphite cores can explain the variation in the bump width, and possible candidates for mantle material are a mixture of neutral polycyclic aromatic hydrocarbons (PAHs) or other forms of non-graphitic carbon (Mathis 1994).

The most striking characteristics of the 2175 Å bumps are the remarkably constant central wavelength, large dispersion of height and width, and variable strength, varying from one line of sight to another (see Fitzpatrick & Massa 2007). The 2175 Å bump in the MW extinction curves appear to be the strongest known to date, though there are very few absolute extinction curves known outside the Local Group. The feature becomes gradually weaker in the LMC and SMC. The two broad categories of LMC sightlines are LMC-average, having MW-type extinction curves, and LMC2 supershell showing weaker bumps and a steep rise into the UV (Nandy et al. 1981; Gordon et al. 2003). The SMC sightlines exhibit a featureless extinction curve and an even steeper rise into the UV. However, a line of sight through the SMC wing exhibits an extinction curve with a prominent 2175 Å bump (Lequeux et al. 1982; Gordon et al. 2003).

The net attenuation curves of local starburst galaxies show that their dust lacks the 2175 Å bump (Calzetti et al. 1994). A significant 2175 Å bump is observed in the spectra of star-forming galaxies at $z \sim 2$, indicating an LMC-like extinction curve (Noll et al. 2007). It has also been detected in the Great Observatories Origins Deep Survey (GOODS)-*Herschel* field galaxies at $z > 1$ (Buat et al. 2011). The detection of the

2175 Å bump has been reported in several individual distant absorbing systems (e.g., Junkkarinen et al. 2004; Wang et al. 2004; Noterdaeme et al. 2009; Zhou et al. 2010; Jiang et al. 2011). The feature has also been detected in the spectral energy distributions (SEDs) of gamma-ray burst (GRB) afterglows with a large diversity of extinction curve shapes (Krühler et al. 2008; Elíasdóttir et al. 2009; Prochaska et al. 2009; Perley et al. 2011; Zafar et al. 2011). The detection of the 2175 Å bump is also reported for an intervening absorber at $z = 1.11$ toward GRB 060418 (Ellison et al. 2006).

GRBs provide a unique tool for studying the absolute extinction curves of distant galaxies because of their bright afterglow emission, simple power-law spectra and their occurrence in star-forming regions. In this paper we report in detail the observations and analyses of two extinguished GRB afterglows showing a 2175 Å bump in their optical spectra: GRB 080605 and GRB 080805, which we compare to the two spectroscopically confirmed 2175 Å bumps in GRB hosts. Previously optical spectra of the afterglows of GRB 080605 and GRB 080805 have been presented in Fynbo et al. (2009) and the SEDs have been discussed briefly in Zafar et al. (2011). Based on photometry, the detection of the bump has also been confirmed for both afterglows (Greiner et al. 2011).

The paper is organized as follows. In Section 2 we describe multi-wavelength observations of the afterglows of GRB 080605 and GRB 080805 carried out with different instruments. In Section 3 we present our results from the SED fitting. In Section 4 we make a comparison between the bump properties of 42 GRB afterglows and Local Group sightlines. We further discuss the extinction curve of GRB 080605. In Section 5 we provide our conclusions.

2. OBSERVATIONS AND DATA REDUCTION

2.1. GRB 080605

Swift Burst Alert Telescope (BAT; Barthelmy et al. 2005) triggered on GRB 080605 on 2008 June 5 at 23:47:57.86 UT. *Swift* X-ray Telescope (XRT; Burrows et al. 2005) slew immediately to the GRB location and began observing the X-ray afterglow of GRB 080605. The Gamma-Ray Optical and Near-Infrared Detector (GROND) observed the field in different optical and NIR bands (Greiner et al. 2011). The afterglow was also observed with the Peters Automatic Infrared Imaging Telescope (PAIRITEL; Bloom et al. 2006) in the *J*, *H*, and *K* bands starting from 5 to 11 and then 31 hr after the burst. The GRB is found close to a bright star, which may contribute to the measured flux. We reduced the PAIRITEL data and used image subtraction techniques (Alard 2000) to get reasonable photometry of the afterglow. To increase the signal-to-noise ratio we stacked the images from 5 to 7 hr and 8 to 11 hr post-burst. The afterglow is clearly detected up to 11 hr after the burst whereas it is not detected at 31 hr after the burst (see Table 1). We also reduced the *Swift* Ultraviolet and Optical Telescope (UVOT; Roming et al. 2005) data of the afterglow. After subtracting the contribution from the nearby object we found that the afterglow is not detected in any of the UVOT bands. The host galaxy of GRB 080605 is bright, with $r' \sim 22.8$ mag (see Krühler et al. 2011) and the contribution is subtracted from the photometric data.

An optical spectrum of the afterglow was secured at the Very Large Telescope (VLT) equipped with the FOcal Reducer and low dispersion Spectrograph 2 (FORS2) using the 300V grism at 3.2 hr (two exposures with an exposure time of 1200 s each) after the burst (Jakobsson et al. 2008b; Fynbo et al. 2009). Spectra were also secured with the 1200R and 1400V grisms yielding a spectral resolution of $R = 2140$ and 2100, respectively. The 300V spectrum was flux calibrated using the spectrum of a spectrophotometric standard star LTT9239 obtained on the same night. The afterglow spectra were taken under good observing conditions. The spectra show several narrow absorption lines with the highest redshift of the absorber at $z_{\rm abs} = 1.6403$, which we adopt as the redshift of the GRB. All photometric and spectroscopic data have been corrected for Galactic extinction using the maps of Schlegel et al. (1998), $E(B-V) = 0.14$ mag.

Lyα absorption could not be detected for this burst with a ground-based telescope due to the relatively low redshift (see Fynbo et al. 2009 for the optical spectrum). A large number of metal species (e.g., Si, C, Al, Zn, Fe, Mg, Mn, and Cr) are identified at the redshift of the GRB (Fynbo et al. 2009). To obtain a limit on the ionic column densities, we analyzed all grism spectra. The absorption features indicate a two-component profile in the 1200R and 1400V spectra. The GRB absorption features are saturated and the resolution is not high enough to estimate reliable limits for the metal column

Table 1
Photometric Observations of the Afterglow of GRB 080605

Mid-time (hr)	Exp. Time (ks)	Instrument	Filters	Magnitudes (AB mag)
0.202	0.02	UVOT	*uvw2*	>19.86
6.158	0.54	UVOT	*uvw2*	>22.52
0.194	0.04	UVOT	*uvm2*	>20.07
8.375	0.26	UVOT	*uvm2*	>22.78
0.201	0.04	UVOT	*uvw1*	>20.41
4.546	0.50	UVOT	*uvw1*	>21.95
0.208	0.04	UVOT	*u*	>20.44
5.160	0.28	UVOT	*u*	>21.20
0.214	0.02	UVOT	*b*	>19.23
7.769	0.58	UVOT	*b*	>20.13
0.113	0.39	UVOT	*v*	18.49 ± 0.10
0.323	0.39	UVOT	*v*	19.37 ± 0.15
6.772	0.24	UVOT	*v*	>19.33
0.042	0.10	UVOT	white	18.87 ± 0.08
0.196	0.10	UVOT	white	20.83 ± 0.19
1.555	0.14	GROND	g'	20.28 ± 0.07
2.785	1.50	GROND	g'	20.76 ± 0.05
1.555	0.14	GROND	r'	19.69 ± 0.06
2.785	1.50	GROND	r'	20.15 ± 0.05
5.512	3.23	GROND	r'	20.68 ± 0.05
6.504	3.23	GROND	r'	20.82 ± 0.06
1.555	0.14	GROND	i'	19.66 ± 0.05
2.785	1.50	GROND	i'	19.66 ± 0.05
1.555	0.14	GROND	z'	18.93 ± 0.07
2.785	1.50	GROND	z'	19.35 ± 0.05
1.555	0.24	GROND	*J*	18.40 ± 0.12
2.785	1.20	GROND	*J*	19.01 ± 0.09
6.021	6.93	PAIRITEL	*J*	19.44 ± 0.22
9.528	9.22	PAIRITEL	*J*	19.39 ± 0.21
1.555	0.24	GROND	*H*	17.99 ± 0.15
2.785	1.20	GROND	*H*	18.56 ± 0.09
6.021	6.93	PAIRITEL	*H*	18.91 ± 0.18
9.528	9.22	PAIRITEL	*H*	19.03 ± 0.19
1.555	0.24	GROND	*K*	17.89 ± 0.23
2.785	1.20	GROND	*K*	18.26 ± 0.11
6.021	6.93	PAIRITEL	*K*	18.93 ± 0.20
9.528	9.22	PAIRITEL	*K*	19.13 ± 0.23

Notes. Magnitudes are given in the AB system, with the host contribution subtracted, and corrected for Galactic extinction of $E(B-V) = 0.14$.

Table 2
Optical/NIR Photometry of the Afterglow of GRB 080805

Time Since Trigger (hr)	Exp. Time (s)	Instrument	Filters	Magnitudes (AB mag)
3.968	1104	UVOT	*uvw2*	>22.91
3.958	415	UVOT	*uvm2*	>21.83
2.248	1082	UVOT	*uvw1*	>22.53
2.404	1081	UVOT	*u*	>22.11
0.283	150	VLT/FORS2	*B*	22.72 ± 0.04
0.719	150	VLT/FORS2	*B*	21.16 ± 0.06
3.102	1082	UVOT	*b*	>21.28
0.080	66	GROND	g'	21.66 ± 0.10
0.243	40	VLT/FORS2	*V*	22.15 ± 0.04
0.679	40	VLT/FORS2	*V*	22.87 ± 0.08
3.331	1207	UVOT	*v*	>20.45
2.513	1180	UVOT	white	>22.87
0.080	66	GROND	r'	20.80 ± 0.08
0.150	30	VLT/FORS2	*R*	20.93 ± 0.02
0.322	30	VLT/FORS2	*R*	21.52 ± 0.03
0.585	30	VLT/FORS2	*R*	21.78 ± 0.04
0.784	10	VLT/FORS2	*R*	22.16 ± 0.09
0.822	10	VLT/FORS2	*R*	22.04 ± 0.08
2.325	120	VLT/FORS2	*R*	22.95 ± 0.06
0.080	66	GROND	i'	20.13 ± 0.08
0.216	40	VLT/FORS2	*I*	20.77 ± 0.02
0.652	40	VLT/FORS2	*I*	21.52 ± 0.05
0.080	66	GROND	z'	19.79 ± 0.08
0.180	60	VLT/FORS2	*z*-Gunn	20.09 ± 0.02
0.616	60	VLT/FORS2	*z*-Gunn	21.00 ± 0.06

Note. Magnitudes are given in the AB system and corrected for Galactic extinction of $E(B-V) = 0.043$.

density. Assuming the Mn II λ2577 line is located at the weak limit of the curve of growth, this would imply that N(Mn II) >13.4 cm^{-2}. The metallicity of the GRB cannot be obtained from the afterglow spectrum due to the absence of a Lyα absorption trough. The metallicity inferred from emission lines from the host is around solar (Krühler et al. 2012). Moreover, the equivalent widths of metal lines are compared with the sample of Fynbo et al. (2009) and Christensen et al. (2011). The equivalent widths of metal lines of GRB 080605 lie above the average for most elements except Fe and Zn. The lower equivalent width for Fe could be due to dust depletion.

2.2. GRB 080805

At 07:41:34.73 UT on 2008 August 05 after the BAT trigger, *Swift* XRT began observations of GRB 080805. GROND observed the afterglow at 4.6 minutes after the burst in the g', r', i', and z' filters. Further imaging of the afterglow were performed with VLT/FORS2 in the Bessel *B*, *V*, *R*, *I*, and *z*-Gunn filters starting from 9 to 139.5 minutes after the burst (see Table 2). VLT/FORS2 photometric data were reduced in standard way. The magnitudes of the afterglow were obtained using ESO zero points from the night of the observation (for *BVRI* filters) and by observing a standard field covered by the Sloan Digital Sky Survey (SDSS) for the *z*-Gunn band. Fitting the *R*-band afterglow light curve provides a temporal index of $\alpha = 0.65 \pm 0.03$ (see Figure 1).

The optical spectrum of the afterglow was taken with VLT/FORS2 (grism 300V) at 1.0 hr (two exposures, each of 600 s) after the burst (Jakobsson et al. 2008a; Fynbo et al. 2009). The spectrum was flux calibrated using the spectrum of a spectrophotometric standard star LTT1020 observed on the same night. The spectra were also obtained with the 1400V, 1200R and 1028z ($R = 2560$) grisms (Jakobsson et al. 2008a). The data were taken under photometric conditions. The UVOT data of the afterglow were reduced and the source was not detected in any of the filters. The redshift is based on a metal system at $z = 1.5042$ displaying Al II λ1671, Fe II λλ2382, 2586, 2600, Mg II λλ2796, 2803 and Mg I λ2852 absorption lines. All data have been corrected for Galactic extinction using the Schlegel et al. (1998) maps with $E(B-V) = 0.043$ mag.

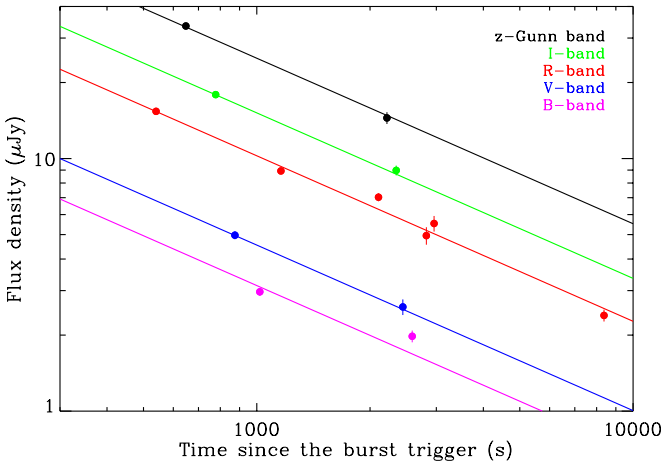

Figure 1. VLT/FORS2 multi-color light curve of the afterglow of GRB 080805. Solid lines are the decay slope of $\alpha = 0.65$, derived from a fit to the *R*-band data. Fluxes are corrected for Galactic extinction of $E(B-V) = 0.043$ mag.
(A color version of this figure is available in the online journal.)

The Lyα absorption line is also not seen for this burst due to its relatively low redshift. Because of the low resolution and highly saturated absorption features, ionic column densities could not be obtained for this burst. We compared equivalent widths of metal lines of this burst with composite samples of Fynbo et al. (2009) and Christensen et al. (2011) and find overabundance in Al and Mg. Fe is about average and this might indicate depletion.

2.3. X-Ray Data

For the two GRB afterglows the *Swift* XRT data were downloaded from the *Swift* data archive. The X-ray data were reduced using HEAsoft (version 6.10). GRB afterglow spectra were extracted in the 0.3–10.0 keV energy range using the latest calibration files. X-ray spectra were obtained near the time of the photometric data. The afterglow light curves were retrieved from the GRB light-curve repository at the UK *Swift* Science Data Centre, created as described in Evans et al. (2010). The light curves were fitted by assuming a smoothly broken power law (Beuermann et al. 1999). Using the light-curve fit, the X-ray spectra were then scaled to the relevant SED time by considering the photon weighted mean time of the X-ray spectra. We used the fitting procedure described in Zafar et al. (2011) where the X-ray spectra are fitted and corrected for soft X-ray absorption below ∼3 keV within XSPEC. The spectrum of GRB 080605 was fitted using a single power law (PL) with a best-fit photon index of $\Gamma = 1.61 \pm 0.19$ and frozen for Galactic X-ray absorption of 6.67×10^{20} cm^{-2} (using the nH FTOOL; Kalberla et al. 2005). The equivalent neutral hydrogen column density from the host galaxy of GRB 080605, estimated from soft X-ray absorption, is $N_{H,X} = 5.58^{+0.44}_{-0.35} \times 10^{21}$ cm^{-2}. The X-ray spectrum of GRB 080805 was fitted with a best-fit photon index of $\Gamma = 1.82^{+0.25}_{-0.22}$ with fixed Galactic absorption

Table 3
Best-fit Extinction Curve Parameters of the Afterglow SEDs Using the FM Parameterization

Parameter	GRB 080605		080805	
t_{SED} (hr)	1.55	2.78	0.08	0.72
c_1	-3.33 ± 1.59	-6.03 ± 0.65	-0.39 ± 1.12	0.09 ± 0.30
c_2 (μm)	1.92 ± 0.55	2.64 ± 0.25	0.63 ± 0.38	0.68 ± 0.14
c_3	1.00 ± 0.68	0.46 ± 0.11	1.39 ± 0.63	$1.10^{+0.51}_{-0.48}$
c_4 (μm^2)	1.27(f)	1.27 ± 0.45	0.40(f)	0.40 ± 0.16
c_5 (μm^{-1})	5.78(f)	5.78 ± 1.03	6.5(f)	6.50 ± 0.27
γ (μm^{-1})	0.82 ± 0.27	0.62 ± 0.07	1.23 ± 1.04	0.91 ± 0.12
R_V	3.24 ± 1.05	$3.19^{+0.86}_{-0.89}$	3.1(f)	3.1(f)
x_0 (μm^{-1})	4.65 ± 0.09	4.53 ± 0.01	4.65 ± 0.05	4.59 ± 0.03
β	0.60 ± 0.03	0.60 ± 0.02	0.80 ± 0.12	0.67 ± 0.03
A_V (mag)	$0.52^{+0.13}_{-0.16}$	$0.50^{+0.13}_{-0.10}$	$2.12^{+0.68}_{-0.63}$	$1.54^{+0.21}_{-0.22}$
χ^2/dof	31/18	733/840	22/11	1268/1317

Notes. The parameters with fixed values are marked (f).

(3.46×10^{20} cm^{-2}). The derived equivalent hydrogen column density is $N_{H,X} = 1.22^{+0.35}_{-0.45} \times 10^{22}$ cm^{-2}.

3. RESULTS

We use a PL or broken power law (BPL) to fit the SEDs and model the extinction with the parameterized extinction curve defined in Fitzpatrick & Massa (1990) consisting of a UV linear component and a Drude component describing the UV/optical extinction curve in the rest frame of the object. In addition we used the c_5 parameter from Fitzpatrick & Massa (2007). We will refer to the extinction model as FM. The parameterized extinction curve for $x > 3.7$ μm^{-1} is written as

$$A_\lambda = A_V \left(\frac{1}{R_V} k(\lambda - V) + 1 \right) \quad (1)$$

where

$$k(\lambda - V) = \begin{cases} c_1 + c_2 x + c_3 D(x, x_0, \gamma) & x \leqslant c_5 \\ c_1 + c_2 x + c_3 D(x, x_0, \gamma) + c_4 (x - c_5)^2 & x > c_5 \end{cases}$$

where $x = \lambda^{-1}$ (μm^{-1}), and the Lorentzian-like Drude profile is expressed as

$$D(x, x_0, \gamma) = \frac{x^2}{\left(x^2 - x_0^2\right)^2 + x^2 \gamma^2} \quad (2)$$

where x_0 is the peak position, γ is the bump width, and c_3 is the bump strength. The UV linear component is controlled by the intercept c_1 and slope c_2. The extinction properties in the optical and infrared ($x < 3.7$ μm^{-1}) are derived using spline interpolation. Additional useful quantities can be defined using the UV parameters, e.g., $A_{\rm bump} = \pi c_3/(2\gamma)$ measures the area of the bump and $E_{\rm bump} = c_3/\gamma^2$ measures the maximum height of the bump above the UV linear extinction (Fitzpatrick & Massa 2007). SEDs of GRB afterglows are modeled with the parameterized extinction curve in the rest frame of the GRB.

We used the uncertainties on the data points to create 1000 Monte Carlo (MC) Gaussian random realizations. We fit these realizations, and in Table 3 we list the standard deviation of this distribution as statistical errors on the best-fit parameters. It should be noted as a caveat that the fitting parameters of the FM model are strongly correlated (see Fitzpatrick & Massa 2007, for a detailed discussion), meaning that the introduction of new data which may change the overall slope for example, also affects the values of many of the other parameters, as observed in the difference between the best-fit parameters here where we have new NIR data, and Zafar et al. (2011) for GRB 080605 without these data. This caution is applicable in this paper especially to GRB 080805 where we have had to assume a value for R_V.

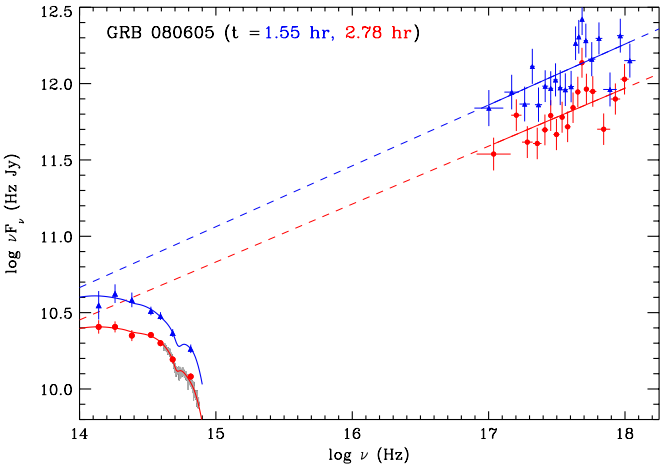

Figure 2. NIR to X-ray SED of the afterglow of GRB 080605 at 1.55 (blue triangles) and 2.78 hr (red circles) after the burst. The gray curve represents the optical spectrum of the afterglow scaled to $t_0 + 2.78$ hr. The solid lines represent the best fits to the data. The dashed lines indicate the unextinguished power laws.

(A color version of this figure is available in the online journal.)

3.1. SED of GRB 080605

The SED of the afterglow of GRB 080605 is extracted at two epochs, i.e., 1.55 and 2.78 hr after the burst (see Figure 2). The GROND-XRT and FORS2/GROND-XRT data were fitted at 1.55 and 2.78 hr, respectively. The FM parameterization is used to fit the afterglow SEDs (see Section 3). The data from both epochs were well fit with a single PL and a 2175 Å bump. The results of the fits are reported in Table 3. The model cannot constrain the c_4 and c_5 parameters at 1.55 hr due to a lack of far-UV data; therefore, the values are fixed to the best-fit value of 2.78 hr. The best-fit parameters from both epochs are all consistent within the 90% interval (see Table 3). The extinction curve from the best-fit model at 2.78 hr is better constrained, and so we use this to examine the extinction properties of the afterglow of GRB 080605 (Figure 3). The extinction curve (in units of A_λ/A_V) of the GRB rises steeply into the UV like the SMC extinction curve but has a significant 2175 Å bump (see Section 4). The $A_{\rm bump}$ at 1.55 hr epoch is $\sim 2\sigma$ significant. We also fit the data with the SMC model of Pei (1992) and found that the model without the bump is not a significantly better fit with an F-test probability of 90% (SMC: χ^2/dof = 53/24, FM: χ^2/dof = 31/18). At 2.78 hr epoch $A_{\rm bump}$ is $\sim 4\sigma$ significant. The derived metals-to-dust ratio based on 2.78 hr epoch results is $N_{H,X}/A_V = 1.12^{+0.16}_{-0.11} \times 10^{22}$ cm^{-2} mag^{-1}.

The FORS2-XRT SED of the afterglow was previously published in Zafar et al. (2011) at 1.74 hr after the burst, finding a large amount of extinction with $A_V = 1.2 \pm 0.1$. Because of the lack of NIR data, the extinction curve was not constrained well in that fit, resulting in a larger A_V and relatively flatter extinction curve (Zafar et al. 2011). Greiner et al. (2011) implemented a GROND-XRT joint fit and found $A_V = 0.47 \pm 0.03$ with the MW dust extinction curve of Pei (1992), similar to the value of A_V found here.

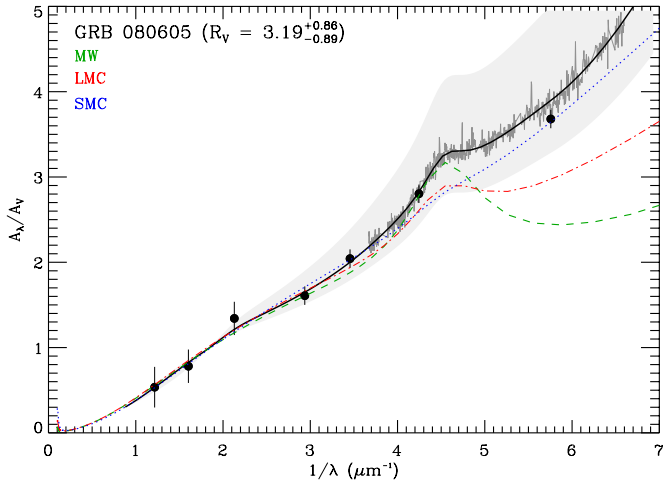

Figure 3. Extinction curve of GRB 080605 using the best-fit model at 2.78 hr after the burst is shown by the black line. The extinction curve is based on the best-fit model given in Table 3. The gray curve represents the optical spectrum. The black circles correspond to the photometric data. The MW (green dashed curve), LMC (red dot-dashed curve), and SMC (blue dotted curve) models from Pei (1992) are also shown. The gray shaded area represents the 1σ uncertainty on the R_V parameter.

(A color version of this figure is available in the online journal.)

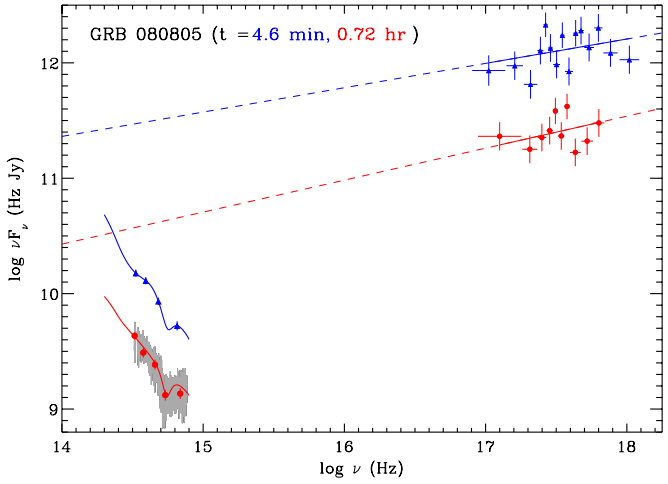

Figure 4. Afterglow SED of GRB 080805 at 4.6 minutes (blue triangles) and 0.72 hr (red circles). The gray curve corresponds to the FORS2 optical spectrum. The solid lines are the best fits to the data. The dashed lines represent the unextinguished power laws.

(A color version of this figure is available in the online journal.)

3.2. SED of GRB 080805

The SED of the afterglow of GRB 080805 was constructed at 4.6 minutes and 0.72 hr after the burst. The GROND-XRT and FORS2-XRT SEDs are well fitted with a single PL and a 2175 Å bump (see Figure 4). The R_V cannot be constrained for this burst because of the lack of NIR data; therefore, the value is fixed to the average value of the MW, i.e., $R_V = 3.1$. Because we do not have a detection in the far-UV at 4.6 minutes after the burst, the c_4 and c_5 fit parameters are fixed to the best-fit value of 0.72 hr epoch results. The $A_{\rm bump}$ at 0.72 hr epoch is $\sim 5\sigma$ significant. At 4.6 minute epoch $A_{\rm bump}$ is $\approx 1\sigma$ significant. Because of less available data in the optical at 4.6 minutes, the significance of the bump cannot confirmed at this epoch. We, therefore, rely mostly on 0.72 hr epoch results for GRB 080805.

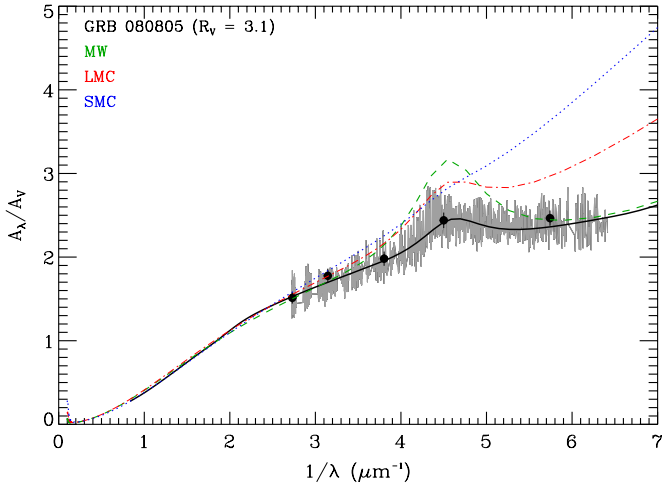

Figure 5. Extinction curve of GRB 080805 using the best-fit model at 0.72 hr after the burst (see Table 3). The optical spectrum is illustrated by the gray curve. The black circles correspond to the photometric observations. The MW (green dashed curve), LMC (red dot-dashed curve), and SMC (blue dotted curve) models from Pei (1992) are also shown.

(A color version of this figure is available in the online journal.)

At 4.6 minutes after the burst Greiner et al. (2011) found that GROND-XRT data fit well with a BPL and Pei (1992) LMC dust model. We determine from the optical spectrum that the bump seen for GRB 080805 is not LMC-like and has smaller strength and width than that of the Pei (1992) LMC bump. We fit the data with the FM extinction model using the 0.72 hr SED best-fit results as an initial guess and found that the SED can be well reproduced by a single PL and required a 2175 Å bump. We also fit the data with the LMC of Pei (1992) model and found that a broken power law is not a significantly better fit with an F-test probability of 83% (PL: $\chi^2/{\rm dof} = 25/16$, BPL: $\chi^2/{\rm dof} = 20/14$).

The extinction curve of the afterglow of GRB 080805 was generated by using the best-fit model obtained at 0.72 hr after the burst (see Figure 5). Due to the lack of rest-frame optical/NIR data the overall slope of the extinction curve is not robust for this burst and can deviate from the one shown in Figure 5, resulting in a smaller or larger A_V. The inferred metals-to-dust ratio based on 0.72 hr epoch results is $N_{H,X}/A_V = 0.79^{+0.24}_{-0.31} \times 10^{22}$ cm^{-2} mag^{-1}. It is also worth noting that the maps of Schlegel et al. (1998) have been confirmed by Dutra et al. (2003) up to $E(B-V) = 0.25$ mag. Assuming an uncertainty of 15% (Schlafly et al. 2010), we find that uncertainty in the Galactic extinction correction does not affect our results for both GRB afterglows and is always smaller than our statistical uncertainties.

3.3. SED Fitting of the GRB Afterglow Sample

In this work, we re-fit the GRB afterglow data published in the spectroscopic sample study of Zafar et al. (2011) with the FM extinction model. This was done to obtain the bump parameters especially c_3 (bump strength) and γ (bump width) to study the 2175 Å bump properties, i.e.: (1) how common the 2175 Å bump is in GRB sightlines, (2) variation in the bump strength, width, and area from one GRB sightline to another, and (3) do the GRB bump properties resemble those found in the Local Group? We fit SEDs of 38 GRB afterglows observed with the VLT/FORS instrument (see Zafar et al. 2011, for the complete list of afterglows). All 38 GRBs in Zafar et al. (2011) prefer an

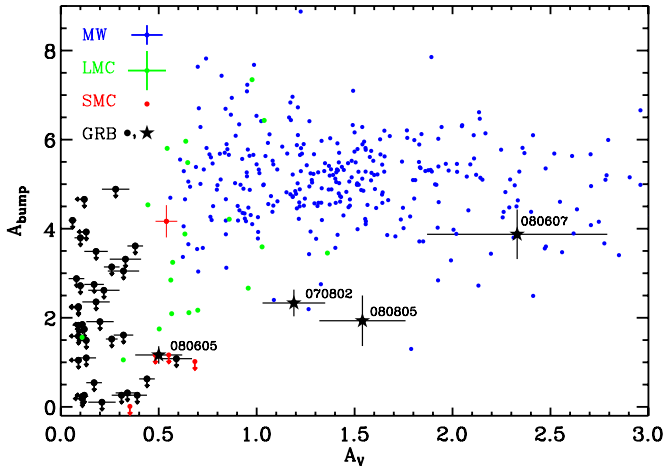

Figure 6. A_{bump} vs. A_V for GRBs, the MW (Fitzpatrick & Massa 2007), LMC, and SMC (Gordon et al. 2003). The black circles indicate the 2σ A_{bump} upper limits for GRBs taken from the sample published in Zafar et al. (2011). The stars represent the GRB afterglows with a detection of the 2175 Å bump in their optical spectra. The blue, green, and red points indicate the MW, LMC, and SMC sightlines, respectively. The green and blue lines on the top-left corner correspond to the average error bars for the LMC and MW data points, respectively.

(A color version of this figure is available in the online journal.)

SMC-type extinction curve. We re-fit those GRBs with the FM extinction model and chose Gordon et al. (2003) mean SMC parameters as an initial guess. From our FM fitting analysis we find that all GRBs with best-fit SMC-type extinction curve in Zafar et al. (2011) have insignificant values of c_3 ($< 3\sigma$). We report 2σ upper limits for c_3 for all 38 afterglows (see Figure 6). GRB 070802 and GRB 080607 are not re-fitted in the current analysis because of having been fit with the FM extinction model in Zafar et al. (2011). We use results for both afterglows from the analysis published in Zafar et al. (2011). GRB 080605 and GRB 080805 are, of course, reviewed in detail in this work and we use results from the current analysis (see Table 3).

4. DISCUSSION

It has previously been found that GRBs reside in low-mass, faint, sub-luminous, and blue galaxies (e.g., Le Floc'h et al. 2003). However, recent studies show that GRBs also occur in a population of dusty, luminous, red, and evolved galaxies (Piro et al. 2001; Levan et al. 2006; Berger et al. 2007; Chen et al. 2010; Krühler et al. 2011). This suggests the previously known faint, young, and low-mass galaxy population is not representative of GRB hosts as a whole. The paucity of the 2175 Å bump found in the afterglows of GRBs to date seems likely to be an indication of our lack of spectroscopic completeness due to dust bias (Zafar et al. 2011) and coincides with the suggestion of Noll et al. (2007) that dust with a significant 2175 Å bump requires an evolved population.

The association between the carriers of the 2175 Å bump and evolved stellar populations would manifest itself also in the host galaxies of the respective GRBs. In comparison to the general population of GRB hosts, these galaxies should have higher stellar masses, higher IR luminosities and global metallicities. Such a trend is indeed observed in recent host samples, which indicate that, on average, galaxies hosting afterglows with a 2175 Å bump are redder, more massive and more luminous than the standard GRB host (Krühler et al. 2011). Similarly, the host of GRB 080605 exhibits high gas-phase metallicity above 0.4 solar which puts it among the most metal-rich GRB hosts ever detected (Krühler et al. 2012). Although number statistics and high-quality host observations are still sparse, the properties of the host galaxies hence seem to support the assertion that the presence of the 2175 Å bump traces environments with evolved stellar populations and substantial chemical enrichment.

Below we compare the results of this analysis to Local Group sightlines to investigate the general properties of the dust in GRB hosts. We discuss the extinction curve of GRB 080605 which is surprisingly different from typical Local Group extinction curves. Cardelli & Clayton (1991) showed that Galactic sightlines could typically be well fit with an R_V-dependent extinction curve. There are a few Galactic sightlines which are not adequately represented by the Cardelli & Clayton (1991) extinction curve (Sofia et al. 2005). We also investigate whether the bump is correlated with the presence of neutral carbon in the gas phase.

4.1. Comparison with Local Group Sightlines

Using the results of the FM fitting analysis, we calculated the area and maximum height of the bump for the GRB afterglow sample of Zafar et al. (2011) by using the relations described above (see Section 3). In Figure 6 we plot A_{bump} against A_V and compare the GRB afterglow sample results to the lines of sight in the MW (Fitzpatrick & Massa 2007), LMC, and SMC (Gordon et al. 2003). We find that A_{bump} (hence the strength and the maximum height of the 2175 Å bump) for the four GRB afterglows with spectroscopically detected 2175 Å bumps is typically smaller than for the vast majority of known Local Group sightlines for a given value of A_V. In other words, the bump for GRB afterglows is not as prominent as in lines of sight in the Local Group. It is interesting to note that it is not simply that the bumps seen in GRB afterglows are weaker and shallower than the bumps seen in the lines of sight in the MW—the extinction curves of GRB afterglows are expected to be different from the MW extinction curves—the bumps are also weaker than those detected in the Magellanic Clouds, where one might expect the dust to be similar, because we are probing actively star-forming environments rather than quiescent regions (see Gordon et al. 2003).

The results of this work imply that the common usage of the average MW, LMC, and SMC extinction models to fit the GRB afterglow SEDs is inadequate (see also Clayton et al. 2000; Gordon et al. 2003). Here we have shown that GRB sightlines with bumps can have weaker bumps than either LMC or MW and bumps in combination with a steep extinction curve, both highly uncharacteristic of most Local Group sightlines. In reality Local Group sightlines exhibit a variety of extinction curves. This work shows that, similar to the Local Group, GRB hosts seem to have a continuum of dust extinction curves varying from steep to flat and bumpy to featureless. In future, better rest-frame UV through NIR data will allow us to obtain reasonable numbers of extinction curves of individual events (see Section 5.2 of Zafar et al. 2011). In support of this objective the X-shooter spectrograph on the VLT is now regularly obtaining UV through NIR spectra of GRB afterglows (e.g., de Ugarte Postigo et al. 2010; D'Elia et al. 2010).

4.2. Dust Composition

The extinction curve of GRB 080605 has a steeper rise into the UV and a weak 2175 Å bump. Such extinction is also seen in the MW in the lines of sight toward HD 210121, and to some extent,

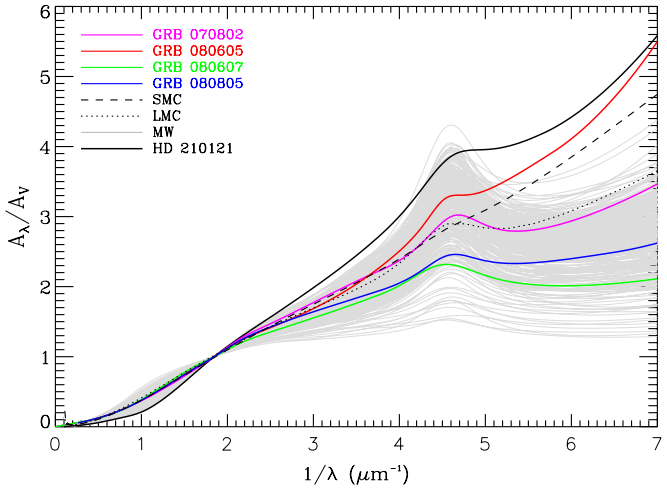

Figure 7. Extinction curves of GRB 070802 (magenta line), GRB 080605 (red line), GRB 080607 (green line) and GRB 080805 (blue line). The SMC and LMC extinction curves taken from Pei (1992) are shown in black dashed and dotted lines, respectively. The black solid line represents the extinction toward the MW star HD 210121. The extinction curves of the MW sightlines taken from (Fitzpatrick & Massa 2007) are shown as gray lines.

(A color version of this figure is available in the online journal.)

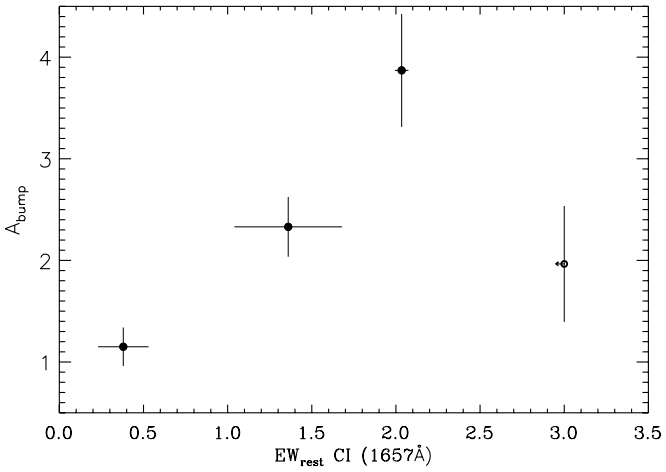

Figure 8. A_{bump} against equivalent width of C I λ1656.9 for GRB afterglows with the 2175 Å bump detected in their optical spectra. The 2σ upper limit for the equivalent width of C I is reported for GRB 080805.

HD 62542 and HD 204827, all of which deviate substantially from the other MW extinction curves (Valencic et al. 2003). The two other interesting extinction curves in the MW are lines of sight toward HD 283809 and HD 29647 showing a weaker bump but a regular flat UV curvature (Clayton et al. 2003; Whittet et al. 2004). Among these, the sightline toward HD 210121 is very unusual, displaying a very steep rise into the far-UV, a small value of $R_V = 2.4$ and a weak 2175 Å bump (Larson et al. 2000; Sofia et al. 2005; see Figure 7). Weingartner & Draine (2001) showed that their carbonaceous/silicate dust model can reproduce the extinction toward HD 210121. They suggested two ways of reproducing the 2175 Å bump: by introducing either small graphite particles or a population of small carbonaceous grains including PAH molecules, and, more likely, the rise into the far-UV may be due to a population of silicate grains (see Weingartner & Draine 2001).

The relative weakness of the GRB afterglow bumps compared to Local Group sightlines hints at the possibility that sightlines with a 2175 Å feature may be composed of two distinct, physically separated dust populations, one with a steep extinction curve and no bump, the other with a relatively flat extinction curve and a strong bump. The steep, featureless curve would then dilute the strength of the bump, and potentially produce the type of extinction curve observed in GRB 080605. In this scenario, both dust populations may reside in the GRB host (e.g., in the molecular cloud in which the GRB forms and in the more general host ISM), or one of the populations in a foreground system. In the case of GRB 070802, for example, we know that there is a foreground absorber at lower redshift with a relatively high metal column density (Elíasdóttir et al. 2009); however, strong dust absorption in foreground systems will not be the typical case. Rather, we have some evidence that two distinct column densities exist in the gas phase within the host galaxy: one nearby and one relatively distant (Perna & Lazzati 2002; Watson et al. 2007; Schady et al. 2011; Vreeswijk et al. 2007; Campana 2009; Krühler et al. 2011). The unusual dust properties observed here may simply be a reflection of this dual population.

4.3. The 2175 Å Bump and C I

The first ionization potential of carbon is 11.3 eV. It is not shielded by neutral hydrogen and hence only expected to be present in regions with a low density of ionizing photons. Carbonaceous materials are believed to be responsible for the 2175 Å bump, and carbonaceous grain growth and formation requires neutral carbon and molecules (Henning & Salama 1998). Therefore it would not be surprising to see both features together from the same environment. In the literature we find two detections of the C I absorption feature in the lines of sight toward the Local Group: (1) the line of sight toward HD 185418 in the MW (Sonnentrucker et al. 2003) and (2) the line of sight toward the SMC-bar with C I detected in the MW but only as an upper limit in the SMC (Welty et al. 1997). Beyond the Local Group, C I absorption is detected in many systems (e.g., Ledoux et al. 2002; Jorgenson et al. 2010). Junkkarinen et al. (2004) reported the detection of the 2175 Å bump for an intervening damped Lyα absorber ($z = 0.524$) toward AO 0235+164 where C I absorption line is also seen (see also Section 4.3 of Elíasdóttir et al. 2009 for more discussion).

To our knowledge C I is detected for all GRB afterglows with a prominent 2175 Å bump except for GRB 080805 due to its low signal-to-noise ratio and redshift. Conversely, C I is also detected in the afterglow spectra of GRB 060210 and GRB 061121 (see Fynbo et al. 2009). However, GRB 060210 is at $z = 3.9133$, so that the bump region is not covered in the optical spectrum. GRB 061121 is at $z = 1.3145$ and has no detection of the 2175 Å bump. The spectra of both afterglows appear to be blue, suggesting little dust extinction for these bursts. We also looked into the spectrum of GRB 060418 which has a reported intervening absorber at $z_{abs} = 1.107$ with a 2175 Å bump. At this redshift C I is blended with the C IV doublet arising from the GRB host galaxy ($z = 1.49$). Fitting the C IV doublet leaves a residual, suggesting the presence of another line, most probably C I from the intervening absorber.

It is striking that the extinguished afterglows with detected C I absorption also have a 2175 Å bump. The presence of C I absorption in the afterglows with the 2175 Å bump suggests that the UV radiation field is weaker in these GRBs. In Figure 8 we attempt to quantify this with the very little data we have. It is possible that there may be a correlation between the area under

the bump and the rest-frame equivalent width of C I λ1656.9. The numbers are too small, however, to confirm any relation. Such a correlation would suggest that we expect to see large equivalent widths of C I for strong bumps and less for weak ones. It should be noted that the ground electronic state of C I split into three fine structure states as C I, C I*, and C I** (see, e.g., Jorgenson et al. 2010). In our low resolution data we cannot distinguish the strength of the various contributions of the excited states. If the C I line is not saturated then the EW of the complex is a useful indication of the column density of neutral carbon. But if the C I line is saturated and in the presence of significant excited states of C I, our EW measurements may not be a meaningful measure of the column density in C I.

We briefly also compared the area of the bump with the underlying UV slope of the GRB extinction curves, i.e., c_2/R_V. We find a hint of a relationship between the two quantities suggesting that smaller C I equivalent widths are observed for GRBs with steeper UV extinction curve slopes and vice versa. In future such relationships can be checked with a larger sample of detected 2175 Å bump and significant C I absorption. If such a correlation holds then C I could be used as a spectroscopic signature to locate the 2175 Å bump in dusty environments.

5. CONCLUSIONS

In this paper, we investigated the 2175 Å bump observed in GRB afterglows. We performed multi-epoch NIR–X-ray SED analysis of GRB 080605 and 080805 displaying 2175 Å bumps in their optical spectra. We find the SEDs to be well fitted with a PL and an FM extinction model at different epochs. So far the bump is spectroscopically detected in the spectra of five GRB afterglows where one is in an intervening absorber. We compare the bump properties of our GRB afterglow sample to Local Group sightlines. We find that $A_{\rm bump}$ for GRB afterglows is smaller for a given A_V than almost all Local Group sightlines. All four GRB extinction curves with detected 2175 Å bumps differ from one another. The differences in the extinction curves suggest that the use of the average MW, LMC, and SMC extinction curve is inadequate. In particular, we know that the extinction curve of the afterglow of GRB 080605 is very different from the other GRB extinction curves, with a 2175 Å bump and steep rise into the far-UV. Such extinction curves and the relative faintness of the bump strength with total extinction might suggest that the dust we observe in the afterglow spectrum consists of two different grain populations having different compositions. The presence of the bump also contradicts the common notion that GRBs occur only in blue, low-mass and faint galaxies. We find a hint of a possible relationship between $A_{\rm bump}$ and neutral carbon for GRB afterglows that needs to be further investigated.

The Dark Cosmology Centre is funded by the Danish National Research Foundation. We are grateful to the anonymous referee for constructive comments. We are thankful to Daniele Malesani, Anja C. Andersen, and Jens Hjorth for helpful discussion. J.P.U.F. acknowledges support from the ERC-StG grant EGGS-278202. G.L. is supported by the Carlsberg foundation. T.K. acknowledges support by the European Commission under the Marie Curie Intra-European Fellowship Programme and support by the DFG cluster of excellence "Origin and Structure of the Universe." This work is based in part on observations done with the European Southern Observatory (ESO) utilizing the 8.2 m VLT, Chile, under program 081.A-0856(B).

REFERENCES

Alard, C. 2000, A&AS, 144, 363
Barthelmy, S. D., Barbier, L. M., Cummings, J. R., et al. 2005, Space Sci. Rev., 120, 143
Berger, E., Fox, D. B., Kulkarni, S. R., Frail, D. A., & Djorgovski, S. G. 2007, ApJ, 660, 504
Beuermann, K., Hessman, F. V., Reinsch, K., et al. 1999, A&A, 352, L26
Bloom, J. S., Starr, D. L., Blake, C. H., Skrutskie, M. F., & Falco, E. E. 2006, in ASP Conf. Ser. 351, Astronomical Data Analysis Software and Systems XV, ed. C. Gabriel, C. Arviset, D. Ponz, & S. Enrique (San Francisco, CA: ASP), 751
Buat, V., Giovannoli, E., Heinis, S., et al. 2011, A&A, 533, A93
Burrows, D. N., Hill, J. E., Nousek, J. A., et al. 2005, Space Sci. Rev., 120, 165
Calzetti, D., Kinney, A. L., & Storchi-Bergmann, T. 1994, ApJ, 429, 582
Campana, S. 2009, ApJ, 699, 1144
Cardelli, J. A., & Clayton, G. C. 1991, AJ, 101, 1021
Chen, H., Perley, D. A., Wilson, C. D., et al. 2010, ApJ, 723, L218
Christensen, L., Fynbo, J. P. U., Prochaska, J. X., et al. 2011, ApJ, 727, 73
Clayton, G. C., Gordon, K. D., Salama, F., et al. 2003, ApJ, 592, 947
Clayton, G. C., Gordon, K. D., & Wolff, M. J. 2000, ApJS, 129, 147
de Ugarte Postigo, A., Goldoni, P., Thöne, C. C., et al. 2010, A&A, 513, A42
D'Elia, V., Fynbo, J. P. U., Covino, S., et al. 2010, A&A, 523, A36
Draine, B. T. 2003, ARA&A, 41, 241
Dutra, C. M., Ahumada, A. V., Clariá, J. J., Bica, E., & Barbuy, B. 2003, A&A, 408, 287
Elíasdóttir, Á., Fynbo, J. P. U., Hjorth, J., et al. 2009, ApJ, 697, 1725
Ellison, S. L., Vreeswijk, P., Ledoux, C., et al. 2006, MNRAS, 372, L38
Evans, P. A., Willingale, R., Osborne, J. P., et al. 2010, A&A, 519, A102
Fitzpatrick, E. L., & Massa, D. 1990, ApJS, 72, 163
Fitzpatrick, E. L., & Massa, D. 2007, ApJ, 663, 320
Fynbo, J. P. U., Jakobsson, P., Prochaska, J. X., et al. 2009, ApJS, 185, 526
Gordon, K. D., Clayton, G. C., Misselt, K. A., Landolt, A. U., & Wolff, M. J. 2003, ApJ, 594, 279
Greiner, J., Krühler, T., Klose, S., et al. 2011, A&A, 526, A30
Henning, T., & Salama, F. 1998, Science, 282, 2204
Henrard, L., Lambin, P., & Lucas, A. A. 1997, ApJ, 487, 719
Jakobsson, P., Fynbo, J. P. U., Vreeswijk, P. M., & de Ugarte Postigo, A. 2008a, GRB Coordinates Network, 8077, 1
Jakobsson, P., Vreeswijk, P. M., Xu, D., & Thoene, C. C. 2008b, GRB Coordinates Network, 7832, 1
Jiang, P., Ge, J., Zhou, H., Wang, J., & Wang, T. 2011, ApJ, 732, 110
Jorgenson, R. A., Wolfe, A. M., & Prochaska, J. X. 2010, ApJ, 722, 460
Junkkarinen, V. T., Cohen, R. D., Beaver, E. A., et al. 2004, ApJ, 614, 658
Kalberla, P. M. W., Burton, W. B., Hartmann, D., et al. 2005, A&A, 440, 775
Krühler, T., Fynbo, J. P. U., Geier, S., et al. 2012, A&A, submitted (arXiv:1203.1919)
Krühler, T., Greiner, J., Schady, P., et al. 2011, A&A, 534, A108
Krühler, T., Küpcü Yoldaş, A., Greiner, J., et al. 2008, ApJ, 685, 376
Larson, K. A., Wolff, M. J., Roberge, W. G., Whittet, D. C. B., & He, L. 2000, ApJ, 532, 1021
Le Floc'h, E., Duc, P.-A., Mirabel, I. F., et al. 2003, A&A, 400, 499
Ledoux, C., Srianand, R., & Petitjean, P. 2002, A&A, 392, 781
Lequeux, J., Maurice, E., Prevot-Burnichon, M., Prevot, L., & Rocca-Volmerange, B. 1982, A&A, 113, L15
Levan, A., Fruchter, A., Rhoads, J., et al. 2006, ApJ, 647, 471
Mathis, J. S. 1994, ApJ, 422, 176
Nandy, K., Morgan, D. H., Willis, A. J., Wilson, R., & Gondhalekar, P. M. 1981, MNRAS, 196, 955
Noll, S., Pierini, D., Pannella, M., & Savaglio, S. 2007, A&A, 472, 455
Noterdaeme, P., Ledoux, C., Srianand, R., Petitjean, P., & Lopez, S. 2009, A&A, 503, 765
Pei, Y. C. 1992, ApJ, 395, 130
Perley, D. A., Morgan, A. N., Updike, A., et al. 2011, AJ, 141, 36
Perna, R., & Lazzati, D. 2002, ApJ, 580, 261
Piro, L., Garmire, G., Garcia, M. R., et al. 2001, ApJ, 558, 442
Prochaska, J. X., Sheffer, Y., Perley, D. A., et al. 2009, ApJ, 691, L27
Roming, P. W. A., Kennedy, T. E., Mason, K. O., et al. 2005, Space Sci. Rev., 120, 95
Schady, P., Savaglio, S., Krühler, T., Greiner, J., & Rau, A. 2011, A&A, 525, A113
Schlafly, E. F., Finkbeiner, D. P., Schlegel, D. J., et al. 2010, ApJ, 725, 1175
Schlegel, D. J., Finkbeiner, D. P., & Davis, M. 1998, ApJ, 500, 525
Sofia, U. J., Wolff, M. J., Rachford, B., et al. 2005, ApJ, 625, 167
Sonnentrucker, P., Friedman, S. D., Welty, D. E., York, D. G., & Snow, T. P. 2003, ApJ, 596, 350
Stecher, T. P. 1965, ApJ, 142, 1683

Steel, T. M., & Duley, W. W. 1987, ApJ, 315, 337
Valencic, L. A., Clayton, G. C., Gordon, K. D., & Smith, T. L. 2003, ApJ, 598, 369
Vreeswijk, P. M., Ledoux, C., Smette, A., et al. 2007, A&A, 468, 83
Wang, J., Hall, P. B., Ge, J., Li, A., & Schneider, D. P. 2004, ApJ, 609, 589
Watson, D., Hjorth, J., Fynbo, J. P. U., et al. 2007, ApJ, 660, L101
Weingartner, J. C., & Draine, B. T. 2001, ApJ, 548, 296
Welty, D. E., Lauroesch, J. T., Blades, J. C., Hobbs, L. M., & York, D. G. 1997, ApJ, 489, 672
Whittet, D. C. B., Shenoy, S. S., Clayton, G. C., & Gordon, K. D. 2004, ApJ, 602, 291
Zafar, T., Watson, D., Fynbo, J. P. U., et al. 2011, A&A, 532, A143
Zhou, H., Ge, J., Lu, H., et al. 2010, ApJ, 708, 742